M. Wörner and G. Grötzbach: "Analysis of the transport equation of temperature variance dissipation rate by direct numerical simulation data of natural convection", pp. 229-238, in: *Engineering Turbulence Modelling and Experiments 3*, Eds.: W. Rodi & G. Bergeles, Elsevier, 1996

Analysis of the transport equation of temperature variance dissipation rate by direct numerical simulation data of natural convection

M. Wörner and G. Grötzbach

Forschungszentrum Karlsruhe, Institut für Reaktorsicherheit,
Postfach 3640, D-76021 Karlsruhe, Germany

Direct numerical simulation data for turbulent Rayleigh-Bénard convection in air and sodium are used to perform an analysis of the transport equation of temperature variance dissipation rate ε_T. The budget of ε_T reveals that at higher turbulence levels the dominant terms are the generation and destruction due to fine scale turbulence interaction. The turbulent diffusion is small but not zero. Therefore, the generation and destruction terms are only approximately in local equilibrium. Our analysis shows that the model commonly used for closure of generation/destruction of ε_T performs reasonably well, while those for turbulent diffusion based on simple gradient assumptions have strong deficiencies.

1. INTRODUCTION

In the past few years great efforts have been devoted to the development of statistical turbulence models which can accurately predict the heat transfer in turbulent buoyant flows for rather universal situations. A recent discussion of the limitations and achievements in modelling and computation of buoyant turbulent flows and heat transfer is presented by Hanjalić [1]. One of his major conclusions is that adequate definition of the turbulent heat flux vector requires the use of both the mechanical and thermal turbulence time scales. Since for most situations the ratio R of these two scales varies appreciably across the flow (see e.g. [2]), Hanjalić recommends that the thermal time scale be determined by solution of transport equations for the temperature variance $\overline{T'^2}$ and its dissipation rate ε_T. However, he emphasizes that the modelled ε_T-equation has to undergo a detailed scrutiny before a standard form for buoyant flows is established.

In the present paper we use results of direct numerical simulations of turbulent convection to perform a detailed analysis of the transport equation for ε_T. By computing each term in the exact equation we evaluate the budget of ε_T and discuss the relative importance of the different terms. In addition, we analyse some models which are commonly used for closure of the ε_T-equation. Thus, the scope of the present contribution is to provide reliable data for the ε_T-equation, to improve the general understanding of different terms in this equation, to point out some deficiencies of current turbulence models, and to suggest some possible improvements. Although we consider a rather simple geometrical and physical application, i.e. the Rayleigh-Bénard convection, and modest turbulence levels we believe that our results are of fundamental interest for the development of reliable and more universal models.

Table 1
Parameter and grid data of simulations

Pr	Ra	Bo	Gr	$X_{1,2}$	$N_{1,2}$	N_3	$\Delta x_{1,2}$	$\Delta x_{3,Wall}$
0.71	630,000	447,300	887,324	7.92	200	49	0.0396	0.005
0.006	24,000	144	4,000,000	8.0	250	49	0.032	0.005

2. PHYSICAL AND NUMERICAL MODEL

2.1. Rayleigh-Bénard convection

This is a process of natural convection developed in a large horizontal fluid layer, which is bounded by rigid walls at top and bottom and is heated from below. The Rayleigh-Bénard convection is characterized by the Prandtl number $Pr = \nu/\kappa$ (where ν = kinematic viscosity, κ = thermal conductivity) and the Rayleigh number $Ra = g\beta\Delta T_W D^3/(\nu\kappa)$ (where g = gravity , β = thermal expansion coefficient, ΔT_W temperature difference between the walls, D = channel height). From Ra and Pr two further dimensionless numbers can be defined: the Grashof number $Gr = Ra/Pr$ and the Boussinesq number $Bo = Ra \cdot Pr$.

In this paper we discuss results of two simulations. In the first one, the fluid is air with $Pr = 0.71$ and $Ra = 630,000$, while in the second simulation the fluid is liquid sodium with $Pr = 0.006$ and $Ra = 24,000$. Thus, the Prandtl number, Rayleigh number and Boussinesq number of both simulations are quite different, see Table 1. However, the Grashof number is of magnitude 10^6 in both cases. Physically, the high values of Gr mean that the velocity field in both simulations is clearly turbulent. In air, where $Bo \approx 4 \cdot 10^5$ the temperature field is highly irregular too. In liquid sodium, the very low value of the Boussinesq number $Bo = 144$ indicates that the temperature field is governed by the high thermal conductivity and thus is predominantly regular.

2.2. Computer code TURBIT

The direct numerical simulations of turbulent Rayleigh-Bénard convection are performed with the TURBIT code [3]. It is based on a finite volume method and solves the full three-dimensional, time dependent conservation equations of mass, momentum and energy in dimensionless form. For normalisation the channel height D, the velocity $\sqrt{g\beta\Delta T_W D}$, and the temperature difference ΔT_W are used. Incorporating the Boussinesq approximation, the governing equations may be summarized for a Cartesian coordinate system as follows:

$$\frac{\partial u_j}{\partial x_j} = 0 \tag{1}$$

$$\frac{\partial u_i}{\partial t} + \frac{\partial (u_i u_j)}{\partial x_j} = -\frac{\partial p}{\partial x_i} + \frac{1}{\sqrt{Gr}} \frac{\partial^2 u_i}{\partial x_j \partial x_j} - (T_{ref} - T)\delta_{i3} \qquad (i = 1, 2, 3) \tag{2}$$

$$\frac{\partial T}{\partial t} + \frac{\partial (T u_j)}{\partial x_j} = \frac{1}{\sqrt{Bo}} \frac{\partial^2 T}{\partial x_j \partial x_j} \tag{3}$$

Here, the summation convention applies and x_1 and x_2 correspond to the horizontal directions and x_3 to the vertical direction. For spatial disretization, a staggered grid

and central finite differences are used. Time integration of the momentum equation is performed by the explicit Euler-Leapfrog scheme, involving the projection method of Chorin to fullfil the conservation of mass. For time advancement of the energy equation, the semi-implicit Leapfrog-Crank-Nicolson scheme is used.

To simulate the semi-infinite fluid layer of the Rayleigh-Bénard convection, periodic boundary conditions are used in both horizontal directions. The corresponding lengths of the channel are chosen to be $X_{1,2} \approx 8D$ and thus they should be large enough to cover even the largest macroscopic scale of the convective layer. At the lower and upper walls, i.e. $x_3 = 0$ and $x_3 = 1$ respectively, the no slip condition and constant wall temperatures are specified. The numbers of mesh cells N_i used in the equidistantly discretized horizontal and non-equidistantly discretized vertical directions are given in Table 1. The resulting mesh widths Δx_i are small enough to resolve the smallest scale of turbulence, while $\Delta x_{3,Wall}$ is sufficient to resolve the boundary layers near the walls.

The simulations with the mesh parameters listed in Table 1 are the last of a series of simulations. Starting from the final data of a simulation with the same Pr but smaller Ra, the results are interpolated to a finer grid and advanced in time. After the flow is fully developed, another interpolation to an even finer grid and additional integration in time is performed until finally a mesh is reached which meets the requirements of a direct numerical simulation. The procedure described drastically reduces the computation time needed to perform the simulations. For a detailed verification of the numerical results by experimental data we refer to [4].

3. RESULTS FOR THE ε_T-EQUATION

3.1. Analysing procedure

In a statistical sense, in turbulent Rayleigh-Bénard convection the physical conditions are homogeneous with respect to the horizontal dimensions. Thus, for evaluation of statistical quantities, averaging is performed over horizontal planes. The resulting vertical profiles $f(x_3)$ are averaged over time, where only data within the fully developed flow regime are used. As a consequence of this averaging procedure, the mean vertical velocity $\overline{u}_3$ is zero and derivatives of statistical quantities with respect to x_1 and x_2 do vanish.

3.2. Temperature variance dissipation rate

Engineering computational methods solve statistically averaged transport equations, closed by turbulence models, which describe turbulent flow and heat transfer. In buoyant flows, the need arises to determine the temperature variance $\overline{T'^2}$ to account for the production/destruction of turbulent heat fluxes by buoyancy forces. Usually, the quantity $\overline{T'^2}/2$ is calculated from its own transport equation. In a recent paper, we used our direct simulation data and performed an analysis of this transport equation [2]. The sink term in the $\overline{T'^2}/2$-equation is the temperature variance dissipation rate ε_T. With the normalisation used here, it is defined as

$$\varepsilon_T = \frac{1}{\sqrt{Bo}} \overline{\frac{\partial T'}{\partial x_j} \frac{\partial T'}{\partial x_j}} \tag{4}$$

In Figure 1 we show the evaluated vertical profiles of ε_T for the simulation with air and sodium. In both cases ε_T is maximum near the walls. In sodium, the variations of ε_T over

the channel height are relatively small. In air the value of ε_T is low in the centre of the channel, while there are sharp peaks near the walls. These differences in the profiles of ε_T in both cases can be related directly to the different characteristics of the temperature fields. In sodium, the profile of $\overline{T}$ is nearly linear and the thermal boundary layers extend almost over the whole channel crossection. For air, a mean temperature profile is found which shows thin boundary layers and an isothermal core, see Figure 2. In the isothermal core region the amplitude of temperature fluctuations and the gradient $\partial T'/\partial x_3$, which appears in definition 4, may be expected to be reduced as compared to the boundary layers, where strong gradients of the mean temperature do exist.

A simple model often used to determine ε_T is [5]

$$\varepsilon_T = \frac{1}{R}\frac{\overline{T'^2}/2}{k}\varepsilon \tag{5}$$

where k is the turbulent kinetic energy and ε is its dissipation rate. In this model, the ratio of mechanical and thermal turbulence time scale R is assumed to be constant. However, for most situations this is a crude approximation, because R depends on Prandtl number and turbulence level, see e.g. [2] and [6]. A more general concept is to determine ε_T by solution of a seperate transport equation.

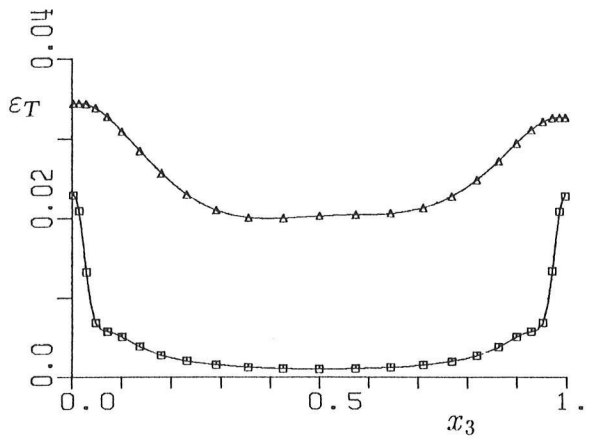

Figure 1. Profiles of ε_T: air(□), sodium(△).

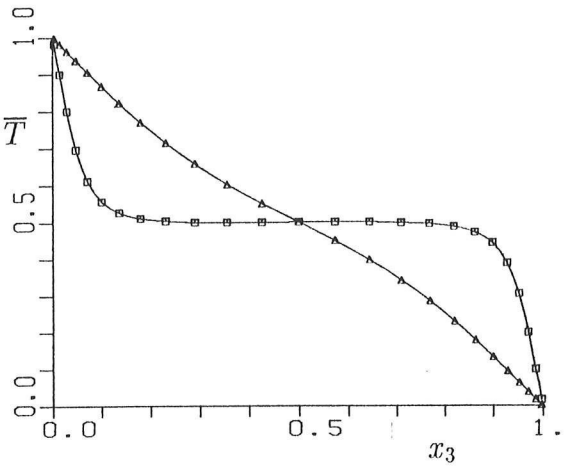

Figure 2. Profiles of $\overline{T}$: air(□), sodium(△).

3.3. Transport equation for ε_T

For Rayleigh-Bénard convection the exact transport equation (see e.g. [6]) for the dimensionless temperature variance dissipation rate ε_T reduces to:

$$\frac{\partial \varepsilon_T}{\partial t} = \underbrace{-\frac{2}{\sqrt{Bo}}\overline{\frac{\partial T'}{\partial x_j}\frac{\partial u_3'}{\partial x_j}}\frac{\partial \overline{T}}{\partial x_3}}_{P^1_{\varepsilon_T}} \underbrace{-\frac{2}{\sqrt{Bo}}\overline{u_3'\frac{\partial T'}{\partial x_3}}\frac{\partial^2 \overline{T}}{\partial x_3 \partial x_3}}_{P^2_{\varepsilon_T}} \underbrace{-\frac{2}{\sqrt{Bo}}\overline{\frac{\partial T'}{\partial x_l}\frac{\partial T'}{\partial x_3}}\frac{\partial \overline{u}_l}{\partial x_3}}_{P^3_{\varepsilon_T}}$$
$$\underbrace{-\frac{2}{\sqrt{Bo}}\overline{\frac{\partial T'}{\partial x_j}\frac{\partial u_l'}{\partial x_j}\frac{\partial T'}{\partial x_l}}}_{P^4_{\varepsilon_T}} \underbrace{-\frac{2}{Bo}\overline{\left(\frac{\partial^2 T'}{\partial x_j \partial x_l}\right)^2}}_{\gamma_{\varepsilon_T}} \underbrace{-\frac{\partial}{\partial x_3}\left(\overline{\varepsilon_T' u_3'} - \frac{1}{\sqrt{Bo}}\frac{\partial \varepsilon_T}{\partial x_3}\right)}_{D_{\varepsilon_T}} \tag{6}$$

Here, $P^1_{\varepsilon_T}, P^2_{\varepsilon_T}$, and $P^3_{\varepsilon_T}$ are generation terms due to the mean temperature and mean velocity field, and $P^4_{\varepsilon_T}$ and γ_{ε_T} are the generation and destruction due to fine scale turbulence interaction. The diffusive transport of ε_T consists of a turbulent and a molecular contribution, i.e. $D_{\varepsilon_T} = D_{\varepsilon_T,t} + D_{\varepsilon_T,m}$. The net contribution of D_{ε_T} to the budget of ε_T is zero, since it only acts as a redistribution term.

3.4. Budget of ε_T

From our direct numerical simulation data, we calculate each term on the right-hand side of equation 6 and evaluate the budget of ε_T. Figure 3 shows the results for the simulation with air, where P_{ε_T} represents the sum of the four generation terms. Different axes of ordinates are used for the lower and upper parts of the channel to yield a better resolution of the various (symmetric) curves. Outside the thermal boundary layers, the

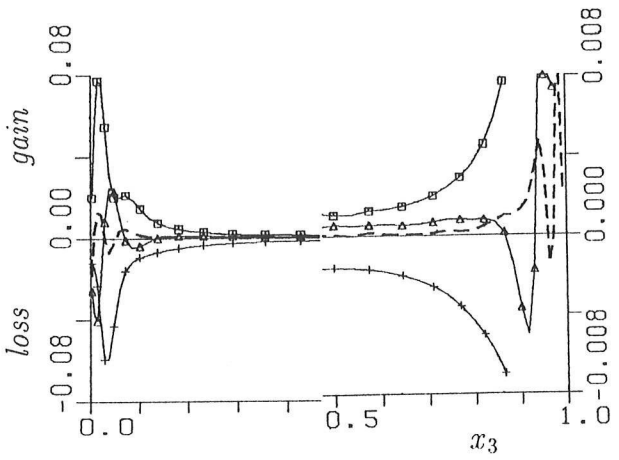

Figure 3. Budget of ε_T for air: P_{ε_T} (□), γ_{ε_T} (+), D_{ε_T} (△), balance difference (- - -).

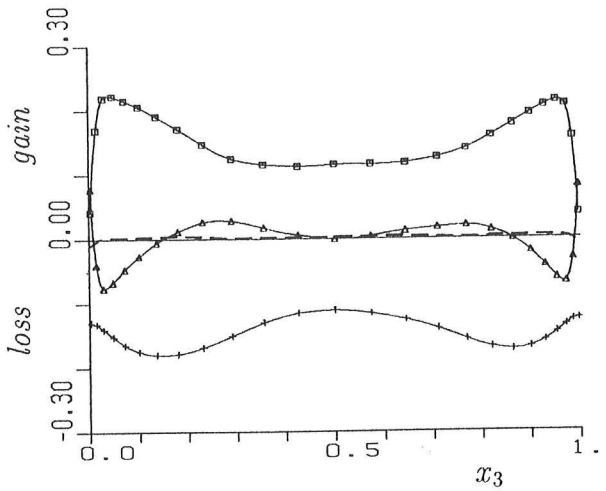

Figure 4. Budget of ε_T for sodium: P_{ε_T} (□), γ_{ε_T} (+), D_{ε_T} (△), balance difference (- - -).

evaluated balance difference (which corresponds to the rate of change of ε_T but also incorporates inaccuracies due to numerical computation of the different balance terms) is very small. In this region, the diffusive transport of ε_T appears as a source term, taking about half the value of P_{ε_T}. Thus, we get the result that the generation and destruction terms are approximately in local equilibrium. Inside the boundary layers, P_{ε_T} and γ_{ε_T} show sharp peaks. Since these peaks occur at somewhat different distances from the walls, the diffusive transport is very important in these regions in balancing the difference between P_{ε_T} and γ_{ε_T} by redistribution of ε_T towards the centre of the channel.

The budget of ε_T for the simulation with sodium is clearly different from that in air, see Figure 4. As the thermal boundary layers extend almost over the whole channel, the profiles of P_{ε_T} and γ_{ε_T} are rather uniform and do not show sharp peaks. The diffusion term D_{ε_T} redistributes ε_T from the regions near walls toward the inner part of the layer, like in the simulation with air.

Figure 5 shows results for the four generation terms for the simulation with air. In the centre of the channel the only important generation term is due to fine scale turbulence interaction $P^4_{\varepsilon_T}$. This result is consistent with the arguments of Launder [6] that at high

Reynolds numbers (i.e. here at high Bo and Gr) the mean-field generation terms are negligible. At the edges of the thermal boundary layers, however, the mean temperature exhibits strong gradients and thus the mean-field generation terms $P^1_{\varepsilon_T}$ and $P^2_{\varepsilon_T}$ become important. Of special interest is the term $P^2_{\varepsilon_T}$ which shows a rather unusual behaviour. Positive values occur at the edges of the thermal boundary layers, indicating generation of ε_T. However, as the wall is approached $P^2_{\varepsilon_T}$ changes sign. Thus, in the direct vicinity of the walls $P^2_{\varepsilon_T}$ acts as a sink term. In turbulent Rayleigh-Bénard convection mean velocities $\overline{u}_i$ are zero and thus the term $P^3_{\varepsilon_T}$ is zero, too.

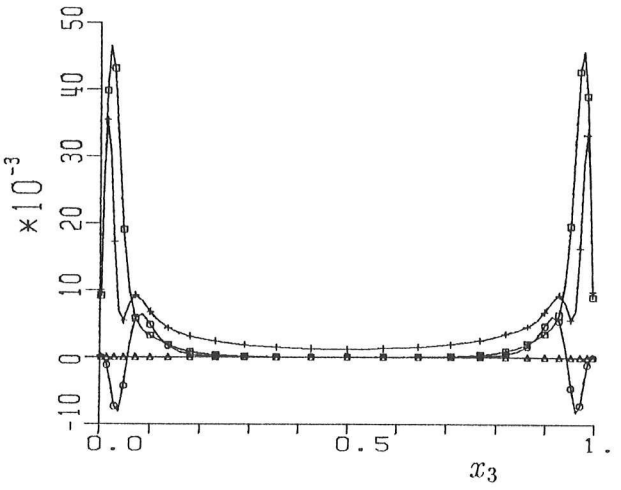

Figure 5. Profiles of $P^1_{\varepsilon_T}(\square)$, $P^2_{\varepsilon_T}(\circ)$, $P^3_{\varepsilon_T}(\triangle)$ and $P^4_{\varepsilon_T}(+)$ for air.

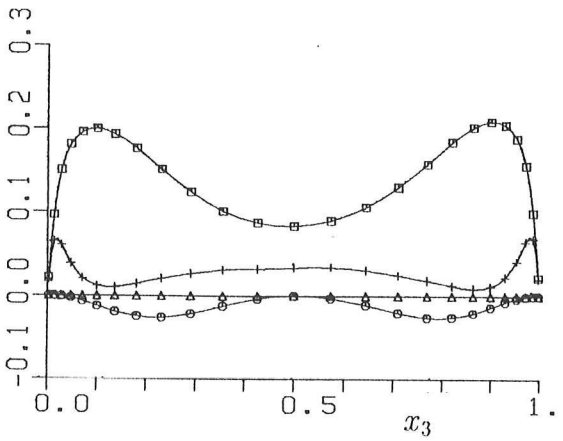

Figure 6. Profiles of $P^1_{\varepsilon_T}(\square)$, $P^2_{\varepsilon_T}(\circ)$, $P^3_{\varepsilon_T}(\triangle)$ and $P^4_{\varepsilon_T}(+)$ for sodium.

The generation terms in sodium are quite different as compared to air, see Figure 6. Because of the low value of Bo, the most important production term is not that due to fine scale turbulence interaction (i.e. $P^4_{\varepsilon_T}$) but is due to the generation by the mean temperature field, i.e. term $P^1_{\varepsilon_T}$. The term $P^2_{\varepsilon_T}$ is now a sink term in the whole layer and does not change sign. As in the simulation with air, $P^3_{\varepsilon_T}$ is zero.

For the simulation with air, the diffusion term $D_{\varepsilon_T,m}$ is zero in the centre of the layer while $D_{\varepsilon_T,t}$ takes a finite value, see Figure 7. Near the walls, where sharp gradients of ε_T exist, $D_{\varepsilon_T,m}$ is one of the dominant terms in the budget of ε_T. For sodium, the diffusive transport of ε_T is dominated in the whole layer by the molecular contribution, see Figure 8. It is interesting to note that in sodium the molecular and turbulent parts of diffusion act in opposite directions.

4. ANALYSIS OF MODEL ASSUMPTIONS

To close the ε_T-equation following terms need to be modelled: the turbulent diffusion $D_{\varepsilon_T,t}$, the generation terms $P^1_{\varepsilon_T}, P^2_{\varepsilon_T}, P^3_{\varepsilon_T}, P^4_{\varepsilon_T}$ and the destruction term γ_{ε_T}. In this section we use our direct simulation data to analyse some model assumptions for these terms which are commonly used in the literature.

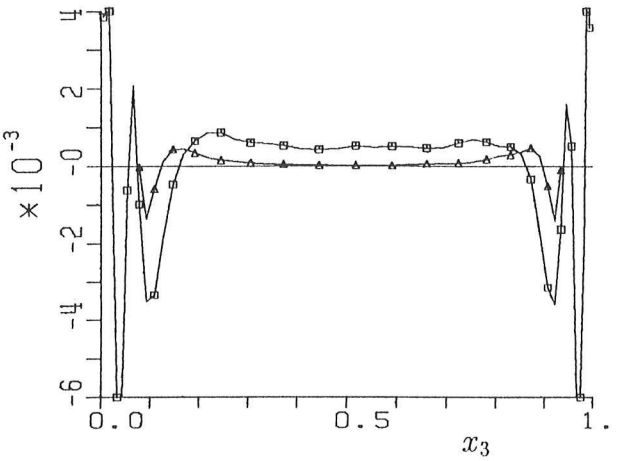

Figure 7. Profiles of $D_{\varepsilon_T,m}(\square)$ and $D_{\varepsilon_T,t}(\triangle)$ for air.

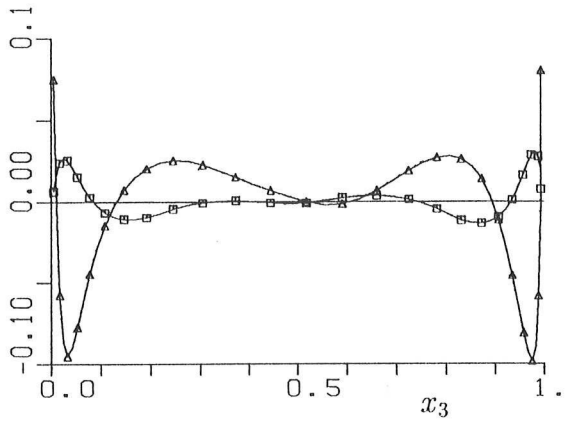

Figure 8. Profiles of $D_{\varepsilon_T,m}(\square)$ and $D_{\varepsilon_T,t}(\triangle)$ for sodium.

4.1. Models for generation and destruction terms of ε_T

Usually, the generation and destruction terms due to fine scale turbulent interaction are modelled together with the mean-field generation terms $P^1_{\varepsilon_T}$ and $P^3_{\varepsilon_T}$ by the following ansatz [7]:

$$P^1_{\varepsilon_T} + P^3_{\varepsilon_T} + P^4_{\varepsilon_T} + \gamma_{\varepsilon_T} = \underbrace{C_{P1} f_{P1} \frac{\varepsilon_T}{\overline{T'^2}} P_T}_{M_1} + \underbrace{C_{P2} f_{P2} \frac{\varepsilon_T}{k} P_k}_{M_2} \underbrace{- C_{D1} f_{D1} \frac{\varepsilon_T^2}{\overline{T'^2}}}_{M_3} \underbrace{- C_{D2} f_{D2} \frac{\varepsilon \varepsilon_T}{k}}_{M_4} \tag{7}$$

Here, in the production terms M_1 and M_2, the term P_T is the production of temperature variance and P_k is the strain production of turbulent kinetic energy:

$$P_T = -\overline{u_j' T'} \cdot \frac{\partial \overline{T}}{\partial x_j} \ , \qquad P_k = -\overline{u_i' u_j'} \cdot \frac{\partial \overline{u_i}}{\partial x_j} \tag{8}$$

In the following, we restrict our attention to the regions outside the boundary layers. Thus we put the wall functions for simplicity to $f_{P1} = f_{P2} = f_{D1} = f_{D2} = 1.0$ and take the following standard values for the coefficients: $C_{P1} = 1.8$, $C_{P2} = 0.72$, $C_{D1} = 2.2$, $C_{D2} = 0.8$ [7]. The results of the evaluated model terms M_1, M_2, M_3, and M_4 are shown in Figure 9 for the simulation with air and in Figure 10 for sodium. Since the mean velocities are zero in Rayleigh-Bénard convection, the evaluated model term M_2 is zero too. In air, in addition, term M_1 vanishes in the isothermal region of the layer. In sodium, where $\partial \overline{T}/\partial x_3$ is finite everywhere, the profile of M_1 shows a plateau. As the sink terms M_3 and M_4 are concerned, we identify for both fluids M_3 as the dominant one in the model of equation 7.

In Figures 11 and 12 we show results for the left-hand and right-hand side of equation 7, where each side is evaluated seperately from our direct simulation data. By this, we investigate how well the model of equation 7 performs for both cases under consideration. As was shown in Figure 3, in air the production and destruction terms are not exactly in local equilibrium. Thus, the evaluated left-hand side of equation 7 is negative in the centre of the layer, see Figure 11. This corresponds to a loss of ε_T which is balanced by

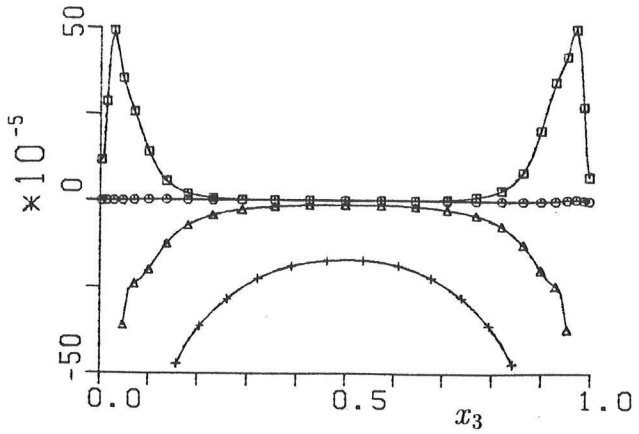

Figure 9. Profiles of $M_1(\square)$, $M_2(\circ)$, $M_3(\triangle)$ and $M_4(+)$ for air.

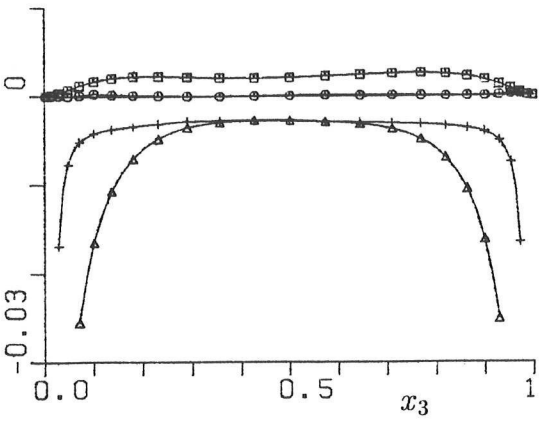

Figure 10. Profiles of $M_1(\square)$, $M_2(\circ)$, $M_3(\triangle)$ and $M_4(+)$ for sodium.

turbulent diffusion (compare with Figure 7). The profile for the sum of the four terms on the right-hand side of equation 7 shows that the model also does not exactly predict local equilibrium. However, the predicted loss of ε_T is much smaller than the actual loss. For sodium a similar conclusion holds for the centre of the layer, see Figure 12.

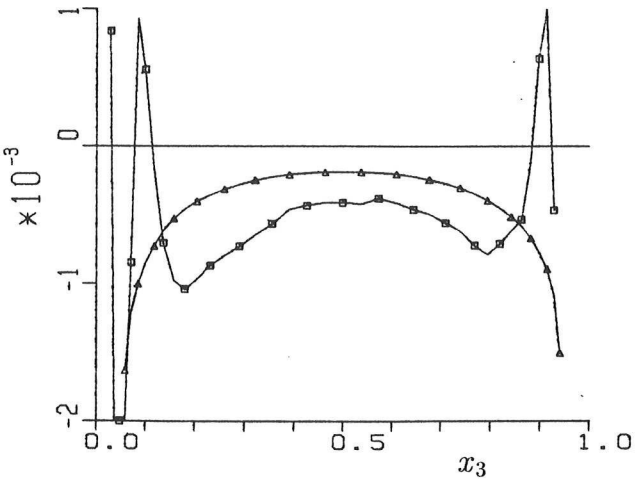

Figure 11. Left-hand side ($\square$) and right-hand side ($\triangle$) of equation 7 for air.

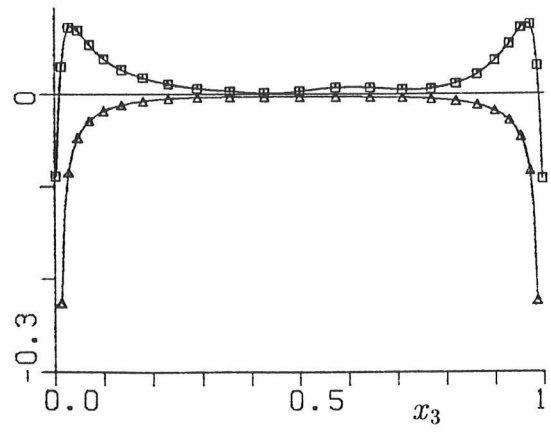

Figure 12. Left-hand side ($\square$) and right-hand side ($\triangle$) of equation 7 for sodium.

For the mean-field generation term $P^2_{\varepsilon_T}$ in equation 6 usually a seperate model is adopted, see e.g. [7]. In the present paper we do not analyse corresponding models but conclude from the results discussed in section 3.4 that in the boundary layers adequate modelling of term $P^2_{\varepsilon_T}$ is of great importance.

4.2. Models for turbulent diffusion of ε_T

The unknown correlation appearing in the turbulent part of the diffusion D_{ε_T} is often modelled by the simple gradient hypothesis [8]

$$\overline{\varepsilon_T' u_i'} = -C_S \frac{k}{\varepsilon} \overline{u_i' u_j'} \frac{\partial \varepsilon_T}{\partial x_j} \tag{9}$$

Sometimes, the tensorial exchange coefficient $k\overline{u_j' u_k'}/\varepsilon$ in equation 9 is replaced by the scalar form k^2/ε, resulting in:

$$\overline{\varepsilon_T' u_i'} = -C_{DD} \frac{k^2}{\varepsilon} \frac{\partial \varepsilon_T}{\partial x_i} \tag{10}$$

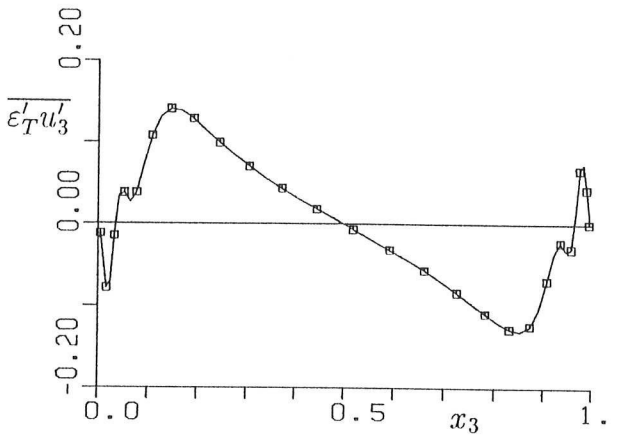

Figure 13. Evaluated profile of $\overline{\varepsilon_T' u_3'}$ for air.

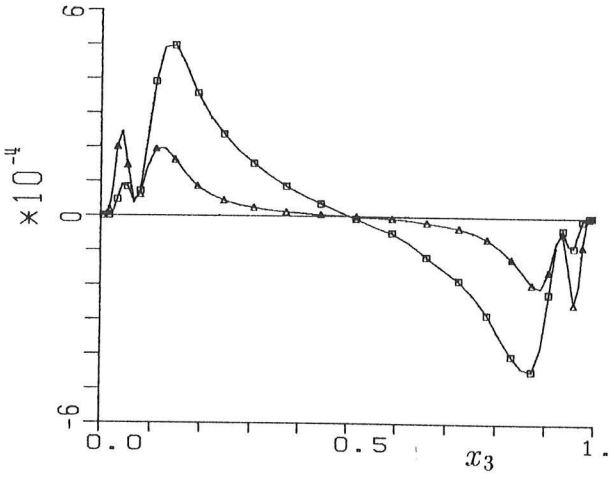

Figure 14. Profile of $\overline{\varepsilon_T' u_3'}$ predicted by model 10 (□) and model 11 (△).

In the following, we compare the correlation $\overline{\varepsilon_T' u_3'}$ predicted by models 9 and 10 with the profile of $\overline{\varepsilon_T' u_3'}$, evaluated from our direct simulation data. For the coefficients we use the values $C_S = 0.22$ and $C_{DD} = 0.03$, respectively. Here, we restrict our discussion to the simulation with air. From a qualitative point of view, the profile of $\overline{\varepsilon_T' u_3'}$ predicted by model 9 (Figure 14) compares quite well with the exact curve (Figure 13). However, quantitatively the diffusion predicted by both models is about 3 orders of magnitude too low. This strong underestimate of turbulent diffusive transport by models 9 and 10 may be of some importance for the simulation considered here where the diffusion term is relatively important. As has been shown in section 3.4, in the centre of the layer it assumes a value of $D_{\varepsilon_T} \approx P_{\varepsilon_T}/2$. At much higher values of Gr and Bo, however, the importance of turbulent diffusion will decrease and the generation/destruction terms may approach really a state of local equilibrium. Nevertheless, the present analysis indicates that simple gradient models are not adequate for physical situations where gradients of statistical quantities are almost zero (i.e here $\partial \varepsilon_T / \partial x_3$).

5. CONCLUSIONS

In this paper we used results of direct numerical simulations of turbulent Rayleigh-Bénard convection in air ($Ra = 630,000$) and sodium ($Ra = 24,000$) and performed a detailed analysis of the transport equation of temperature variance dissipation rate ε_T.

The analysed budget of ε_T showed that in the simulation with air, where the convection is clearly turbulent, the dominant terms are the generation and destruction due to fine scale turbulence interaction. In this case the mean-field generation terms are only of importance in the boundary layers, where strong gradients of mean temperature exist. At the turbulence level considered, the turbulent diffusive transport of ε_T is still of some importance and the generation/destruction terms are only approximately in local equilibrium. In sodium, where the velocity field is turbulent while the temperature field is governed by thermal diffusion, the production of ε_T is mainly due to mean-field generation, not due to fine scale turbulence interaction.

The numerical results are used to scrutinize models commonly used in literature for closure of the ε_T-equation. Focusing our attention to regions far from walls, the model for the generation/destruction terms in the ε_T-equation is found to perform reasonably well. However, the model predicts a state which is much closer to local equilibrium than it is found in the direct simulation. In modelling the turbulent diffusion of ε_T, simple gradient models are found to be inadequate. As in most parts of the channel the spatial gradient of ε_T is about zero such models strongly underestimate the diffusive transport. This failure of gradient diffusion models may not be of special relevance at much higher turbulence levels than considered here, where for the generation and destruction terms a state of local equilibrium may really be expected to exist. Nevertheless, there is a strong need for a reliable diffusion model which is not based on a gradient assumption.

ACKNOWLEDGEMENT

Sincere thanks go to Mrs. A. Hennemuth, who developed the subroutines for analysis of the ε_T-equation.

REFERENCES

1. K. Hanjalić, Proc. 10th Int. Heat Transfer Conf., Brighton, U.K., Vol. 1 (1994) 1.
2. M. Wörner and G. Grötzbach, Proc. ICHMT Int. Symposium on Turbulence, Heat and Mass Transfer, Lisbon, Portugal, Vol. 1 (1994) 9.3.1.
3. G. Grötzbach, in: *Encyclopedia of Fluid Mechanics,* Ed.: N.P. Cheremisinoff, Gulf Publ., Houston, **6** (1987) 1337.
4. M. Wörner, Dissertation Universität Karlsruhe, (1994) KfK 5228.
5. B.E. Launder, J. Fluid Mech., **67** (1975) 569.
6. B.E. Launder, in: *Topics Appl. Phys.*, Ed.: P. Bradshaw, Springer, **12** (1976) 231.
7. Y. Nagano and C. Kim, J. Heat Transfer, **110** (1988) 583.
8. W.P. Jones and P. Musonge, Phys. Fluids, **31** (1988) 3589.